Broadband and unidirectional plasmonic hyperlensing in drift-biased graphene 🐵

Cite as: Appl. Phys. Lett. 118, 091107 (2021); https://doi.org/10.1063/5.0042580 Submitted: 31 December 2020 . Accepted: 22 February 2021 . Published Online: 05 March 2021

N. K. Paul, and D J. S. Gomez-Diaz

COLLECTIONS

Note: This Paper is part of the APL Special Collection on Metastructures: From Physics to Applications.



EP This paper was selected as an Editor's Pick













Broadband and unidirectional plasmonic hyperlensing in drift-biased graphene •

Cite as: Appl. Phys. Lett. **118**, 091107 (2021); doi: 10.1063/5.0042580 Submitted: 31 December 2020 · Accepted: 22 February 2021 · Published Online: 5 March 2021







N. K. Paul and J. S. Gomez-Diaza) (1)

Department of Electrical and Computer Engineering, University of California Davis, One Shields Avenue, Kemper Hall 2039, Davis, California 95616, USA

Note: This Paper is part of the APL Special Collection on Metastructures: From Physics to Applications. a) Author to whom correspondence should be addressed: jsgomez@ucdavis.edu

ABSTRACT

AFFILIATIONS

We suggest and explore the possibility to realize broadband and unidirectional plasmonic hyperlensing over a graphene layer biased with two orthogonal drift-biases. This platform relies on the interplay between nonlocality and nonreciprocity to generate ultraconfined states in the direction aligned with the effective biasing current. The presence of these states shapes, elongates, and significantly flattens the isofrequency contour of the supported modes and enforces the canalization of surface plasmons along the two directions defined by the applied biases. Through a dedicated anisotropic Green's function formalism that takes graphene's intrinsic nonlocality into account, we show that this platform resolves the presence of two point-source emitters with a resolution larger than $\lambda_0/500$ over a broad frequency range ($\sim 10-25$ THz) using realistic biasing schemes. We also discuss how spin-orbit interactions can be exploited to construct unidirectional hyperlenses for near-field images with specific polarization distribution. Our findings may open exciting applications in dynamic, subdiffractive, and planar sensing and imaging systems and in the exciting, routing, and processing of surface plasmons.

Published under license by AIP Publishing. https://doi.org/10.1063/5.0042580

Hyperlenses operating in the canalization regime have surpassed the diffraction limit of light, enabling subwavelength imaging 1-4 and finding a wide variety of applications in microscopy, medicine, biology, and physics. These devices transform evanescent harmonics into propagative ones and transfer them all from the near to the far field with identical phase velocity, avoiding diffraction and the loss of subwavelength details contained in higher-order spatial waves. The main challenge to achieve canalization is the design of electromagnetic devices that exhibit an isofrequency contour (IFC)-i.e., the surface momentum space at a constant wavelength—with an elongated flat shape, a configuration that enforces all spatial harmonics to propagate with an identical wavenumber toward a fixed and unique direction.^{5–7} Common implementations able to exhibit such a response include wire media,8 hyperbolic metamaterial structures made of stacking dielectric and metallic layers, 8-12 and epsilon-near-zero metamaterials with extreme anisotropy in the loss (i.e., $Im[\bar{\epsilon}]$), ^{13,14} among many others. 15,16 Recently, there has been increasing interest in translating canalization concepts from bulk three-dimensional configurations to ultrathin plasmonic metasurfaces, 17-19 aiming to achieve deeply subwavelength imaging by exploiting the confined properties of surface plasmon polaritons (SPPs).²⁰ To this purpose, the electric dyadic

conductivity that characterizes passive, nonmagnetic, and reciprocal metasurfaces must be carefully engineered. This can be accomplished, for instance, transferring a graphene layer on top of the nanotriangular-ridge ground plane and exploiting graphene's field effect, taking advantage of the intrinsic properties of certain types of 2D materials 7,22,23 or adequately nanopatterning ultrathin materials at the nanoscale. Unfortunately, these approaches are inherently narrowband, suffer from the presence of loss, and usually require complex implementations. An alternative approach to obtain collimated plasmons relies on using magnetized plasmonic materials, a narrowband platform that requires a magnetic biasing field and is not compatible with modern technology trends.

In a related context, drift-biased graphene has emerged as a promising platform for broadband nonreciprocal plasmonics. ^{26–29} SPPs are collective charge oscillations coupled to light, and thus, they are strongly influenced by drifting charges moving on the interface in which they propagate. As a result, SPPs can effectively see different media when they travel along or against drifting charges. ²⁹ In graphene, ³⁰ this response is remarkably robust because this 2D material simultaneously provides an ultrahigh electron mobility that enables drift velocities very close to the Fermi velocity ($\nu_F \approx 10^6 \, \mathrm{ms}^{-1}$) ^{31–33}

and a strong plasmonic response in the terahertz (THz) and infrared (IR) bands. 34,35 Merging drift-biased graphene with the rich functionalities and strong light-matter interactions provided by patterned metasurfaces has opened new routes to manipulate the states supported by the device, allowing new degrees of freedom to tailor its dispersion diagram (2D IFC) and to excite and steer broadband SPPs immune to backscattering. 29

In this contribution, we explore the possibilities enabled by driftbiased graphene to tailor the IFC of the supported modes and apply it to construct broadband and unidirectional plasmonic hyperlenses. Using a dedicated Green's function formalism and taking the intrinsic nonlocal response of graphene into account,²⁹ we investigate the capabilities of this platform to resolve the presence of two sources located in the near field in terms of subwavelength resolution and operation frequency. We also determine the velocity that drifting electrons must acquire to achieve a desired response. In addition, instead of combining drifting electrons with a nanopatterned structure,²⁹ we apply two longitudinal DC voltages on the graphene sheet to generate drifting electrons moving in orthogonal directions (Fig. 1). This technique avoids the need of nanopatterning the 2D layer or its ground plane and permits us to engineer nonreciprocal, broadband, dynamic, and flat modal dispersions that canalize surface plasmons toward desired directions in the plane. We then exploit the orthogonality between the voltage sources and drifting electrons to generate effectively superluminal currents traveling diagonally along the surface and explore the potential response of such a platform with our semi-classical formalism. Even though the feasibility of a superluminal drift regime in graphene is not yet determined, our results suggest that it would significantly enhance the platform performance. Finally, we take advantage of spin-orbit interactions 36-40 to construct broadband and unidirectional planar hyperlenses for near-field sources with specific field polarization distribution.

The proposed platform is illustrated in Fig. 1(a). It consists of a graphene sheet embedded in hexagonal boron nitride (hBN) and biased with two longitudinal and orthogonal dc voltages (V_{dc}^x and V_{dc}^y) that induce drifting electrons flowing along the \hat{x} and \hat{y} directions with velocities v_d^x and v_d^y , respectively. The nonlocal conductivity that describes this graphene layer can be approximated as 27,29

$$\sigma_d(\omega, v_d^x, v_d^y, k_x, k_y) \approx \frac{\omega}{\omega - k_x v_d^x - k_y v_d^y} \sigma_g(\omega - k_x v_d^x - k_y v_d^y), \quad (1)$$

where $\omega = 2\pi f$ is the oscillation frequency, k_y and k_x correspond to the y and x wavevector components, and σ_g is graphene's conductivity computed using a nonlocal approach. 41,42 Equation (1) accounts for a drift-induced Doppler shift in the momentum space proportional to the velocity of the drifting electrons ($\sim k_x v_d^x + k_y v_d^y$) as well as a negative Landau damping expressed through the factor $\frac{\omega}{\omega - k_x v_y^2 - k_y v_y^2}$ that might lead to plasmon amplification.²⁷ In addition, Eq. (1) assumes that orthogonal drift currents on a graphene layer do not interact with each other. This approach is similar to drift-bias graphene with an effective drift velocity $\overline{v}_d = v_d^x \hat{x} + v_d^y \hat{y} = v_d \hat{e}_c$, where \hat{e}_c is the unit vector that defines the current direction within the plane but allows additional flexibility to manipulate the direction and strength of the effective drift current in a realistic platform by tuning the applied voltage biases. Incorporating Eq. (1) into the nonlocal and anisotropic Green's function framework developed in Ref. 29 permits us to calculate the modal dispersion of drift-biased graphene and its electromagnetic response to point sources. Figure 1(b) shows the IFC of the supported modes for several biasing conditions. In the absence of any drift bias, graphene exhibits an isotropic response associated with transverse-magnetic (TM) surface plasmons (black line). Applying a longitudinal bias along the \hat{x} -axis induces drifting electrons on graphene, which breaks the symmetry of the eigenstates and leads to an effectively anisotropic and nonreciprocal modal response. In the case of drifting electrons with velocity $v_d^x = 0.65v_F$ (blue line), SPPs propagating along the drift (positive k_x half space) travel significantly faster than other modes, exhibiting a moderate field confinement and low loss. On the contrary, SPPs propagating against the drift (negative k_x half space) are extremely confined and lossy, in such a way that they can barely be excited in realistic scenarios. The resulting IFC acquires a closed elliptical shape that is symmetric with respect to the direction orthogonal to the drift axis (i.e., \hat{y}) and whose center has been shifted in the momentum space toward the direction opposite to the drift. Applying an additional drift bias of similar magnitude in the \hat{y} direction [red line in Fig. 1(b)] permits us to further manipulate the supported states by (i) decreasing the field confinement and loss of certain states and (ii) flattening the IFC along the directions of the applied bias. This response arises due to the interplay between nonlocality and nonreciprocity: the effective drift bias generates a strong nonreciprocal response, whereas nonlocality^{41,42} imposes that SPPs must be supported in all directions within the plane. The ultraconfined states that

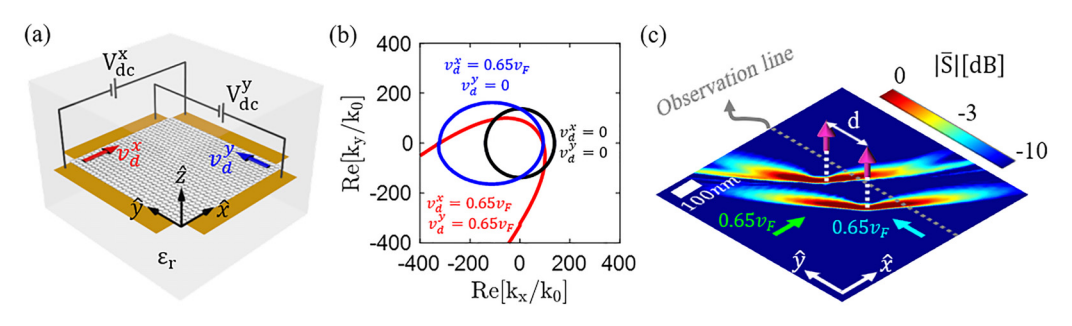


FIG. 1. Proposed planar hyperlensing platform based on drift-biased graphene. (a) Schematic. A graphene sheet embedded in hBN is electrically biased with two longitudinal dc voltages, V_{dc}^x and V_{dc}^y , which generate orthogonal drifting electrons moving along the \hat{x} and \hat{y} axes with velocities v_d^x and v_d^y , respectively. (b) Influence of the drifting electron velocity on the isofrequency contour of the structure. (Black) No bias; (blue) $\bar{v}_d = 0.65v_F \hat{x} + 0.0 \hat{y}$; (red) $\bar{v}_d = 0.65v_F \hat{x} + 0.65v_F \hat{y}$. (c) Excitation of surface waves (normalized magnitude of the Poynting vector \bar{S} in dB) by two \hat{z} -oriented dipoles separated by a distance $d = \lambda_0/100$ (λ_0 is the wavelength) along the \hat{y} axis and located at 15 nm over the surface. The operation frequency is 15 THz, and graphene's chemical potential and relaxation time are set to 0.1 eV and 0.5 ps.

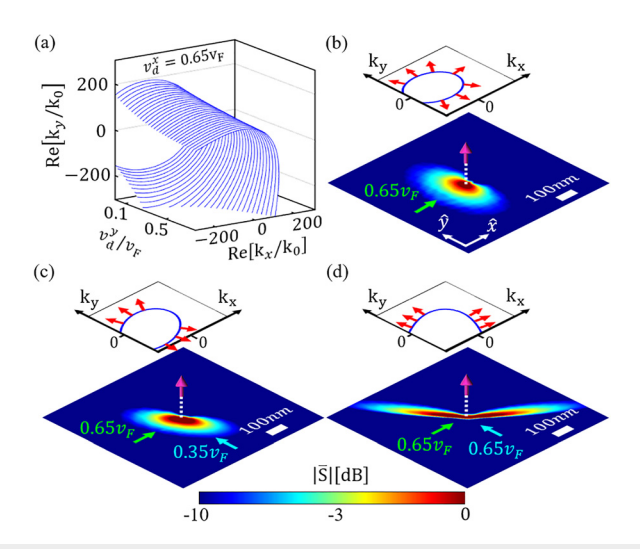


FIG. 2. Properties of the surface plasmons supported by a graphene layer biased with a drift velocity of $v_d^x = 0.65v_F$ along the \hat{x} axis vs the velocity of drifting electrons flowing along the orthogonal direction \hat{y} , $v_{d.}^y$ (a) Isofrequency contour. (b)–(d) Normalized magnitude of the Poynting vector S (in dB) excited by a \hat{z} -oriented dipole located at 15 nm above the surface. Results are computed on the metasurface for (b) $v_d^y = 0$, (c) $v_d^y = 0.35v_F$, and (d) $v_d^y = 0.65v_F$. Each panel contains an inset illustrating the metasurface isofrequency contour and the direction of energy flow (red arrow). Other parameters are as in Fig. 1.

appear in directions opposite to the effective drift elongate and significantly flatten the IFC of the device, thus enabling the use of driftbiased graphene to canalize SPPs. It is important to remark the key role played by nonlocality in determining the platform dispersion and the direction of energy flow: if this phenomenon is not considered, the IFC would exhibit an open shape in the momentum space, which would prevent the propagation of SPPs in directions opposite to the drifting electrons. The strong influence of nonlocality in drift-biased graphene plasmonics is in full agreement with recent works that have discussed how nonlocal effects prevent the presence of truly unidirectional plasmons at homogeneous magnetic interfaces 43-45 by closing the IFC. To illustrate the application of the proposed platform in hyperlensing, Fig. 1(c) shows the excitation of surface waves by two z-oriented dipoles separated by a distance $d = 200 \,\mathrm{nm} \ (\sim \lambda_0 / 100,$ where λ_0 is the free space wavelength) along the \hat{y} axis and located 15 nm over the graphene surface. Results show that SPPs are excited only along directions close to those defined by the applied bias and they travel without any apparent diffraction, demonstrating strong capability for subwavelength imaging. Remarkably, the platform provides a strong nonreciprocal response and prevents any wave propagation in the surface but collimated plasmonic beams. In the following, we investigate the performance of this platform in terms of applied drift bias, resolution, operation frequency, and polarization.

Figure 2 shows the properties of SPPs supported by a graphene layer that is biased with a drift velocity of $v_d^x = 0.65v_F$ along the \hat{x} -axis vs the velocity of drifting electrons traveling toward the orthogonal direction, v_d^y . Specifically, Fig. 2(a) shows the evolution of the IFC in the momentum space vs v_d^y . Results show the capability of this platform to manipulate the IFC in a dynamic manner by adjusting the voltages applied to the orthogonal DC sources. For sufficiently larger values of the drift velocity ($v_d^{\nu} > 0.6v_F$), the IFC acquires the quasi-flat response typical of media operating in the canalization regime. Figures 2(b)-2(d) show the normalized magnitude of the Poynting vector excited by a z-oriented dipole located at 15 nm above the graphene layer when it is biased with different drift velocities. In the different panels, the insets show the IFC of the surface and the direction of energy flow (red arrows). Results clearly illustrate how the quality of the canalization (inversely proportional to the plasmon beam width) and propagation distance of the excited SPPs significantly increase with the velocity of the drifting electrons flowing along the \hat{y} direction, in full agreement with the qualitative analysis of the IFC.

One of the most remarkable properties of the proposed hyperlensing platform is its broadband response, covering from the THz/ far-IR band to the mid-IR. Figure 3(a) shows the IFC of the supported modes from 5 to 25 THz, a frequency region in which intraband contributions dominate the electromagnetic response of graphene. Results show that flat IFCs, associated with strong canalization responses, appear over a very broad frequency region (roughly from 11 to 25 THz). Figures 3(b) and 3(c) further confirm this response, showing the normalized magnitude of the Poynting vector on the drift-biased graphene layer when it is excited by a z-oriented emitter oscillating at 18 and 25 THz, respectively. It should be noted that strong canalization responses are not found at frequencies lower than 10 THz, which we attribute to the lower confinement and larger loss of SPPs supported in this band. However, it might be possible to achieve canalization in these frequencies by increasing the graphene quality (using relaxation times >0.75 ps)⁴⁶ or reducing the chemical potential, which,

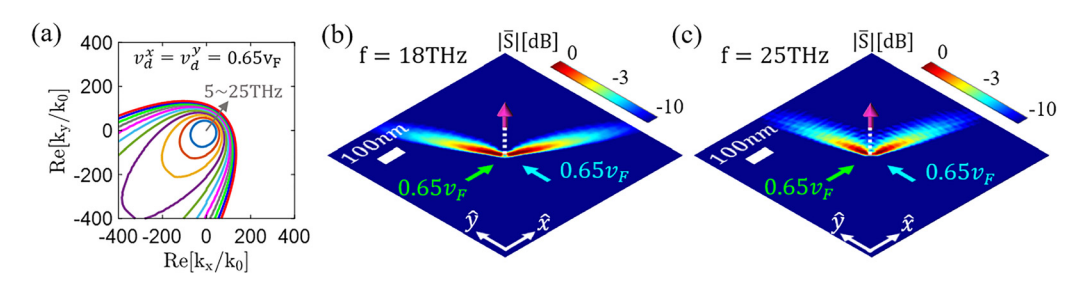


FIG. 3. Broadband response of the proposed planar hyperlensing platform. The structure is biased with a drift velocity of $\bar{v}_d = 0.65v_F \hat{x} + 0.65v_F \hat{y}$. (a) Isofrequency contour at different frequencies. (b) and (c) Normalized magnitude of the Poynting vector \bar{S} (in dB) excited by a \hat{z} -oriented dipole located at 15 nm above the surface. Results are computed on the metasurface at (b) 18 THz and (c) 25 THz. Other parameters are as in Fig. 1.

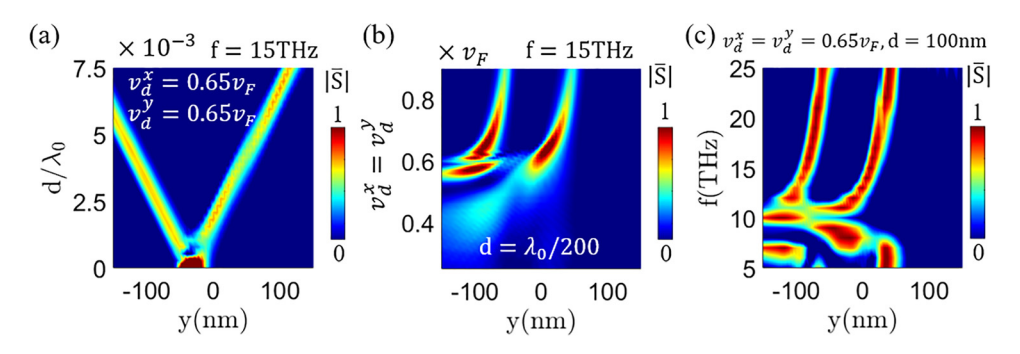


FIG. 4. Performance the proposed planar hyperlensing platform. Results show the normalized magnitude of the Poynting vector \overline{S} (in dB) excited by two \hat{z} -oriented dipoles separated by a subwavelength distance d along the \hat{y} axis computed at a distance of $x_0 = 50$ nm [gray observation line in Fig. 1(c)] vs (a) separation distance d, keeping $\overline{v}_d = 0.65v_F\hat{x} + 0.65v_F\hat{y}$ and f = 15 THz; (b) drift velocity $\overline{v}_d = v_d^x\hat{x} + v_d^y\hat{y}$, keeping $v_d^x = v_d^y$, $v_d^x =$

in turn, would adjust the overall frequency region in which plasmon canalization is supported.

Figure 4 investigates and determines the capability of drift-biased graphene to resolve the presence of emitters separated by deeply subwavelength distances. Specifically, we consider the scenario shown in Fig. 1(c) and study the power of the SPPs excited by two emitters at a fixed distance from them $[x_0 = 50 \text{ nm}, \text{ observation line in Fig. 1(c)}]$ vs the (a) separation distance d between the sources, (b) applied drift velocity, and (c) operation frequency. The performance of the platform is remarkable: it offers resolution larger than ${\sim}\lambda_0/500$ and enables ultrasubwavelength imaging; requires realistic drift velocities $(v_d^x = v_d^y = 0.65v_F \text{ and } |\overline{v}_d| \approx 0.92v_F)$ that have already been experimentally demonstrated in hBN encapsulated graphene;^{31–33} and can easily resolve the presence of emitters separated by 100 nm that oscillate from 12 to 25 THz. Such a response can be enhanced further by increasing the applied orthogonal bias voltages [see Fig. 4(b)] up to a point in which the platform may become superluminal in the sense that the effective drifting electrons move faster than the electron Fermi velocity (i.e., $|\overline{v}_d| > v_F$). In this scenario, electrons move orthogonally along the \hat{x} and \hat{y} axes with a velocity slower than v_F and generate an electromagnetic response similar to the one created by an effectively superluminal motion of electrons drifting diagonally along the metasurface. Although an effectively superluminal regime has not yet been experimentally realized in graphene, we consider this regime as a theoretical possibility and explore its potential performance. Figure 5 shows the hyperlensing response of the platform when it is biased with an effective current $\overline{\nu}_d = 0.8 \nu_F \hat{x} + 0.8 \nu_F \hat{y}$ ($|\overline{\nu}_d| \approx 1.13 \nu_F$). Results confirm the presence of extremely canalized surface plasmons as well as a subwavelength resolution $> \lambda_0/1800$ over a large bandwidth. Even though not studied here for the sake of space, it should be noted that these properties can be further tuned by applying a gate bias, allowing a dynamic control of the hyperlens performance.

The intrinsic nonreciprocal response of drift-biased graphene can be exploited in this platform to put forward unidirectional hyperlenses. To this purpose, one can exploit spin–orbit interactions 36,37,39,40,47 and match the field polarization spin of dipolar sources or a field distribution image with the transverse spin of a subset of modes supported by drift-bias graphene, thus enabling plasmon canalization toward a unique direction within the plane. This possibility is explored in Fig. 6, which shows the excitation of surface waves by two closely located, circularly polarized emitters. Results show that sources with an out-of-plane dipole moment spin rotating along the \hat{x} -axis ($\bar{p} = \hat{x} + i\hat{z} [C \cdot m]$) excite SPPs canalized along the \hat{x} -axis, whereas sources with a spin rotating along the \hat{y} -axis ($\bar{p} = \hat{y} + i\hat{z} [C \cdot m]$) excite SPPs canalized toward the orthogonal direction, \hat{y} . It should be stressed that the spin locking does not deteriorate the overall

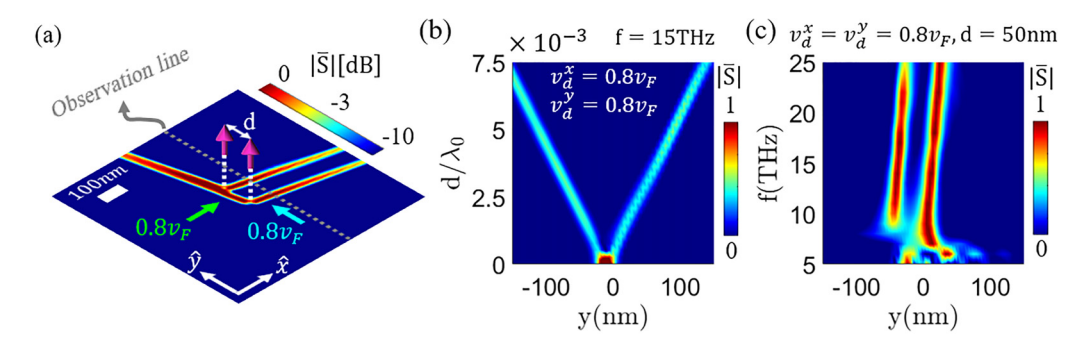


FIG. 5. Performance of the hyperlensing platform in a superluminal case. Graphene is biased with an effective drift current $\bar{v}_d = 0.8v_F \hat{x} + 0.8v_F \hat{y}$ ($|\bar{v}_d| \approx 1.13v_F$). (a) Excitation of surface waves (magnitude of the Poynting vector \bar{S} in dB) by two \hat{z} -oriented dipoles separated by a distance $d = \lambda_0/200$ along the \hat{y} axis and located at 15 nm over the surface. (b) and (c) Response of the platform computed at a distance of $x_0 = 50$ nm [gray observation line panel (a)] vs (b) separation distance d, keeping f = 15 THz and (c) frequency, keeping the separation distance as d = 50 nm. Other parameters are as in Fig. 1.

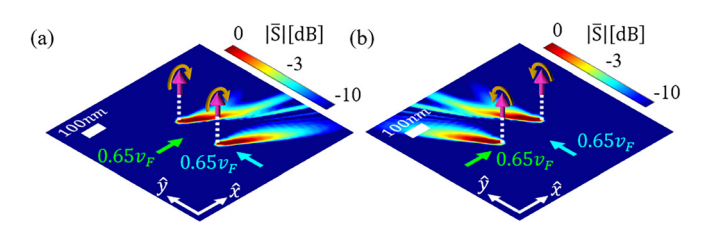


FIG. 6. Unidirectional hyperlensing exploiting the photonic spin Hall effect. Normalized magnitude of the Poynting vector \overline{S} (in dB) excited by two circularly polarized dipoles separated by a distance $d=\lambda_0/100$ and located at 15 nm over the surface. Results are computed on the metasurface at 15 THz when the emitters have a dipole moment with an out-of-plane polarization spin defined by (a) $\overline{p}=\hat{x}+i\hat{z},$ rotating along the \hat{x} -axis and (b) $\overline{p}=\hat{y}+i\hat{z},$ along the \hat{y} -axis. Other parameters are as in Fig. 1.

performance of the hyperlensing platform, which maintains its response in terms of resolution and bandwidth.

In summary, we have put forward a platform to achieve broadband and unidirectional plasmon hyperlensing based on a graphene layer longitudinally biased with two orthogonal dc-voltages. This approach exploits the interplay between nonreciprocity and nonlocality to flatten the isofrequency contour of the supported modes and enable canalization of SPPs toward the direction defined by the applied bias. The proposed platform merges nonreciprocal and canalization responses over a simple structure, avoiding the presence of magnetic bias or the need of nanostructured surfaces, and exhibits a remarkable response in terms of resolution (up to $\sim \lambda_0/1000$) and broadband response (roughly from 10 to 25 THz, keeping a resolution larger than $\lambda_0/500$ in the entire range) while requiring realistic drift bias. Besides, unidirectional canalization can be achieved using emitters or field images with an out-of-plane polarization spin that rotates against the desired direction of propagation. The platform response is tunable with a gate bias, which might lead to a dynamic control and steering of canalized plasmons. In terms of practical implementation, it should be stressed that recent experiments have demonstrated graphene embedded in hBN supporting drift currents with velocities very close to the Fermi velocity ($v_d \approx 0.95v_F$) at room temperature, a response enabled by the reduced carrier scattering with surface optical phonons in hBN. We envision that the unidirectional hyperlensing may trigger exciting applications in subdiffractive imaging, sensing, as well as the excitation, routing, and processing of plasmons over a broad frequency range.

This work was supported by the National Science Foundation with Grant No. ECCS-1808400 and CAREER Grant No. ECCS-1749177.

DATA AVAILABILITY

The data that support the findings of this study are available from the corresponding author upon reasonable request.

REFERENCES

- ¹E. E. Narimanov and V. M. Shalaev, Nature **447**, 266 (2007).
- ²P. Ikonen, P. A. Belov, C. R. Simovski, and S. I. Maslovski, Phys. Rev. B 73, 073102 (2006).
- ³A. Salandrino and N. Engheta, Phys. Rev. B 74, 075103 (2006).
- ⁴Z. Jacob, L. V. Alekseyev, and E. Narimanov, Opt. Express 14, 8247 (2006).

- ⁵D. Correas-Serrano, A. Alù, and J. S. Gomez-Diaz, Phys. Rev. B **96**, 075436 (2017).
- ⁶P. A. Belov, C. R. Simovski, and P. Ikonen, Phys. Rev. B 71, 193105 (2005).
- ⁷D. Correas-Serrano, J. S. Gomez-Diaz, A. A. Melcon, and A. Alù, J. Opt. 18, 104006 (2016).
- ⁸C. R. Simovski, P. A. Belov, A. V. Atrashchenko, and Y. S. Kivshar, Adv. Mater. 24, 4229–4248 (2012).
- ⁹Z. Liu, H. Lee, Y. Xiong, C. Sun, and X. Zhang, Science 315, 1686–1686
- ¹⁰I. I. Smolyaninov, Y. J. Hung, and C. C. Davis, Science **315**, 1699–1701 (2007).
- ¹¹W. Cai, D. A. Genov, and V. M. Shalaev, Phys. Rev. B **72**, 193101 (2005).
- ¹²P. A. Belov and Y. Hao, Phys. Rev. B **73**, 113110 (2006).
- ¹³S. Feng, Phys. Rev. Lett. **108**, 193904 (2012).
- ¹⁴L. Sun, S. Feng, and X. Yang, Appl. Phys. Lett. **101**, 241101 (2012).
- ¹⁵S. A. Ramakrishna, J. B. Pendry, M. C. K. Wiltshire, and W. J. Stewart, J. Mod. Opt. **50**, 1419–1430 (2003).
- ¹⁶P. A. Belov, Y. Zhao, S. Tse, P. Ikonen, M. G. Silveirinha, C. R. Simovski, S. Tretyakov, Y. Hao, and C. Parini, Phys. Rev. B 77, 193108 (2008).
- ¹⁷A. V. Kildishev, A. Boltasseva, and V. M. Shalaev, Science **339**, 1232009 (2013).
- N. Yu and F. Capasso, Nat. Mater. 13, 139–150 (2014).
 W. T. Chen, A. Y. Zhu, and F. Capasso, Nat. Rev. Mater. 5, 604–620 (2020).
- ²⁰S. A. Maier, *Plasmonics: Fundamentals and Applications* (Springer Science & Business Media, 2007).
- ²¹E. Forati, G. W. Hanson, A. B. Yakovlev, and A. Alu, Phys. Rev. B 89, 081410 (2014).
- ²²J. S. Gomez-Diaz, M. Tymchenko, and A. Alù, Opt. Mater. Express 5, 2313–2329 (2015).
- ²³J. S. Gomez-Diaz and A. Alu, ACS Photonics 3, 2211–2224 (2016).
- ²⁴A. A. High, R. C. Devlin, A. Dibos, M. Polking, D. S. Wild, J. Perczel, N. P. De Leon, M. D. Lukin, and H. Park, Nature 522, 192–196 (2015).
- ²⁵S. A. H. Gangaraj, G. W. Hanson, M. J. Silveirinha, K. Shastri, M. Antezza, and F. Monticone, Phys. Rev. B 99, 245414 (2019).
- ²⁶T. A. Morgado and M. G. Silveirinha, ACS Photonics 5, 4253–4258 (2018).
- ²⁷T. A. Morgado and M. G. Silveirinha, Phys. Rev. Lett. **119**, 133901 (2017).
- ²⁸T. A. Morgado and M. G. Silveirinha, Phys. Rev. B **102**, 075102 (2020).
- ²⁹D. Correas-Serrano and J. S. Gomez-Diaz, Phys. Rev. B 100, 081410 (2019).
 ³⁰A. C. Neto, F. Guinea, N. M. Peres, K. S. Novoselov, and A. K. Geim, Rev.
- ³⁰A. C. Neto, F. Guinea, N. M. Peres, K. S. Novoselov, and A. K. Geim, Rev. Mod. Phys. 81, 109 (2009).
- ³¹V. E. Dorgan, A. Behnam, H. J. Conley, K. I. Bolotin, and E. Pop, Nano Lett. 13, 4581 (2013).
- ³²H. Ramamoorthy, E. Somphonsane, J. Radice, G. He, C. P. Kwan, and J. P. Bird, Nano Lett. 16, 399 (2016).
- 33M. A. Yamoah, W. Yang, and E. Pop, ACS Nano 11, 9914 (2017).
- ³⁴A. N. Grigorenko, M. Polini, and K. S. Novoselov, Nat. Photonics 6, 749–758 (2012).
- **35**F. J. Garcia de Abajo, ACS Photonics **1**, 135–152 (2014).
- ³⁶K. Y. Bliokh, F. J. Rodríguez-Fortuño, F. Nori, and A. V. Zayats, Nat. Photonics 9, 796 (2015).
- ³⁷F. Cardano and L. Marrucci, Nat. Photonics 9, 776 (2015).
- ³⁸F. J. Rodríguez-Fortuño, N. Engheta, A. Martínez, and A. V. Zayats, Nat. Commun. 6, 8799 (2015).
- ⁵⁹F. J. Rodríguez-Fortuño, G. Marino, P. Ginzburg, D. O'Connor, A. Martínez, G. A. Wurtz, and A. V. Zayats, Science 340, 328 (2013).
- ⁴⁰K. Y. Bliokh, D. Smirnova, and F. Nori, Science **348**, 1448 (2015).
- ⁴¹D. Correas-Serrano, J. S. Gomez-Diaz, M. Tymchenko, and A. Alù, Opt. Express 23, 29434–29448 (2015).
- ⁴²G. Lovat, G. W. Hanson, R. Araneo, and P. Burghignoli, Phys. Rev. B 87, 115429 (2013).
- ⁴³S. Buddhiraju, Y. Shi, A. Song, C. Wojcik, M. Minkov, I. A. Williamson, A. Dutt, and S. Fan, Nat. Commun. 11, 1–6 (2020).
- 44S. A. Mann, D. L. Sounas, and A. Alu, Optica 6, 104-110 (2019).
- 45 S. A. H. Gangaraj and F. Monticone, Optica 6, 1158–1165 (2019).
- ⁴⁶C. R. Dean, A. F. Young, I. Meric, C. Lee, L. Wang, S. Sorgenfrei, K. Watanabe, T. Taniguchi, P. Kim, K. L. Shepard, and J. Hone, Nat. Nanotechnol. 5, 722–726 (2010).
- ⁴⁷T. Jungwirth, J. Wunderlich, and K. Olejník, Nat. Mater. 11, 382-390 (2012).